Ecological Informatics 78 (2023) 102351

Contents lists available at ScienceDirect

Ecological Informatics

journal homepage: www.elsevier.com/locate/ecolinf

How do conservation policies, climate and socioeconomic changes impact Hyrcanian forests of northern Iran?

Vahid Nasiri [a,b,*], Hadi Beygi Heidarlou [c], Ahmad Abbasnezhad Alchin [d], Fardin Moradi [d], Soroor Rahmanian [e], Samaneh Afshari [d], Carmen Maftei [a], Verena C. Griess [f]

[a] Faculty of Civil Engineering, Transilvania University of Brasov, 900152, Brasov, Romania
[b] Department of Forest Resources Management, Faculty of Forestry, University of Agriculture in Krakow, Krakow, Poland
[c] Forestry Department, Faculty of Natural Resources, Urmia University, P.O. Box 165, Urmia, Iran
[d] Department of Forestry and Forest Economics, Faculty of Natural Resources, University of Tehran, Karaj 1417643184, Iran
[e] German Centre for Integrative Biodiversity Research (iDiv) Halle-Jena- Leipzig, Puschstr. 4, Leipzig 04103, Germany
[f] Department of Environmental Systems Science, Institute of Terrestrial Ecosystems, ETH, Zurich 8092 Zurich, Switzerland

ARTICLE INFO

Keywords:
Conservation policies
Climate change
Forest cover dynamics
Google earth engine
Stepwise multilevel logistic regression

ABSTRACT

Sustainable forest management (SFM) practices are required to conserve forest ecosystem services. International agreements and national management plans have been developed to avoid deforestation and increase forest sustainability. Due to the high rate of deforestation and its increasing trend in the past, the most important conservation policy (the Forest Rest Plan) in Hyrcanian forests (HFs) has been in place since 2016 to conserve the HFs, which are a UNESCO World Heritage site. The aim of the Forest Rest Plan (FRP) is to increase the crown cover, resilience, and production of HFs. Here, we apply a robust methodology based on Landsat-8-derived spectral-temporal features, spatial analysis, stepwise multilevel logistic regression, and scientific forest management knowledge to determine how the FRP, climate change, anthropogenic activities, and the environmental conditions influence deforestation and forest recovery. We identified and evaluated 18 explanatory variables, including socioeconomic, climatic, and physiographic factors, to determine the key drivers of forest cover change. Our findings revealed complex interactions between distinct land features that occur at multiple spatial and temporal scales in HFs as connected human–natural systems. Further, we found a decreasing trend in deforestation and a growing trend in forest recovery resulting from implementation of the FRP. Additionally, our stepwise multilevel logistic regression identified impacts of climate change, human pressure, and some physiographic factors, such as forest density, on deforestation and forest recovery. We conclude that while some positive impacts can already be identified, additional adaptive, preventative, and restorative strategies must be developed to reach all FRP objectives.

1. Introduction

Forests provide essential ecosystem services, such as soil and water preservation (Stritih et al., 2021), biodiversity conversation (Rahmanian et al., 2021), and air quality improvement (Başkent, 2021). Sustainable forest management (SFM) entails developing forest management practices that assure the provision of environmental, social, and economic benefits while meeting a variety of forest needs (Hu et al., 2022). Currently, forestry communities and policymakers face the challenging task of designing and implementing SFM-based strategies due to the escalating forest disturbances caused by factors such as population growth, climate change, insect outbreaks, diseases, and wildfires (Santos et al., 2022). The international research community has provided evidence that rates of forest degradation and deforestation have increased across various biomes in recent decades (Yuh et al., 2023). According to earlier studies, the conversion of forests to other land uses (Beygi Heidarlou et al., 2023), illegal logging and related trade (Lynch et al., 2013), and inappropriate management practices such as clear-cutting for mining activities and infrastructure development (Silva Junior et al., 2021) are the most important drivers of deforestation. Chakraborty et al. (2017) also mentioned in their research that deforestation is a major global concern due to climate change and biodiversity

* Corresponding author at: Faculty of Civil Engineering, Transilvania University of Brasov, 900152, Brasov, Romania.
E-mail addresses: vahid.nasiri@unitbv.ro (V. Nasiri), h.beygi@urmia.ac.ir (H.B. Heidarlou), soroor.rahmanian@unitbv.ro (S. Rahmanian), s.afshari@ut.ac.ir (S. Afshari), carmen.maftei@unitbv.ro (C. Maftei), verena.griess@usys.ethz.ch (V.C. Griess).

https://doi.org/10.1016/j.ecoinf.2023.102351
Received 3 May 2023; Received in revised form 22 October 2023; Accepted 22 October 2023
Available online 25 October 2023

conservation. The growing awareness of carbon emissions caused by forest degradation, deforestation, and land-use/land-cover change (LULCC) has resulted in the establishment of international agreements and frameworks, such as REDD+ (Reducing Emissions from Deforestation and Forest Degradation), that establish clear political priorities for preventive actions and outline prevention strategies.

However, persistent forest degradation and deforestation show that these initiatives have not delivered the desired results (Sotirov et al., 2020). In addition to international forest agreements, national and regional policies and legislations have a significant effect on forest conservation, and they could be even more effective if they were tightly linked with international forest policies and developed and implemented in accordance with international obligations (Scullion et al., 2019).

Currently, many national strategies primarily focus on implementing bans on logging and clear-cutting. The success of these strategies varies widely among countries and depends on the socio-economic, cultural, and political framework, as well as on environmental preconditions and how the strategies are implemented. For example, China banned the cutting of trees from natural forests from 1998 to 2020 using a stepwise approach, starting in the Yangtze River watershed and subsequently extending throughout the northeastern provinces. According to the most recent data, forest logging in 2016–2020 decreased by 6.3% (volume of logged wood) compared with values in 2010–2015, demonstrating the effectiveness of this management strategy (Tong et al., 2020). As another example, the federal government of Pakistan established a nationwide ban on commercial timber harvesting between 1990 and 1992, and a master plan for forestry development (MPFD) was then implemented from 1993 to 2018, with the aims to promote commercial plantations and afforestations and to expand protected areas (Ahmad et al., 2022). Previous research found this strategy to be ineffectual. However, illicit harvesting and trade expanded in response to growing demand, while legitimate harvesting and marketing fell (Fischer and Project, 2010).

Iran, a country deficient in forests (6.8% forested), is also facing severe deforestation. Hyrcanian forests (HFs) are the main source of industrial timber in Iran, whereas the rest of the forests, including Zagros forests, Iran-Touranian forests, Arasbarani forests, and the Persian Gulf and Sea of Oman regions, are not harvested commercially due to low growth rates and vulnerability to deforestation and forest degradation. Over the last several decades, there have been substantial changes in legislation, planning, and strategy governing HFs policies and management practices. The first stage involved stopping clear-cutting on a large scale in restoration regions, the second involved converting even-aged stands to uneven-aged stands, and the third involved spot-cutting in a handful of selected locations (Jourgholami and Majnounian, 2011). Although all these management strategies were aimed at reducing the harvesting pressure on HFs, they all allowed forests to be commercially used until 2016. In 2016 the Iranian Parliament approved a new management plan, the Forest Rest Plan (FRP), banning all exploitation and commercial harvesting in HFs, with the goal to improve forest cover, resilience, and productivity. Due to the FRP, none of the harvesting contracts were renewed, which resulted in significant adjustments to management procedures. As a result, forest exploitation contracts have been steadily revoked since 2016, and forest harvesting is now fully illegal, as are forest exploitation plans. Only restoration management plans and forest conservation policies are now being implemented for HFs, including those supporting afforestation and combatting timber smuggling and forest conversion to other land uses.

To evaluate the success of any forest management strategy or policy, long-term monitoring and inventory systems are required. Such monitoring can reveal strategies to regulate and increase ecological connectedness across forest zones, and so manage the landscape as a coherent system (Hassan et al., 2023; Morley et al., 2018). The regular assessment of the development of forest resources in an area of question makes it possible to track changes regarding forest resources, forest health, and the forest's capacity to provide ecosystem services. Such information forms the basis for reviewing policy and management processes, their effectiveness, and their outcomes (Coops et al., 2023). In addition to monitoring deforestation and forest recovery rates caused by a new management policy, the impact of other drivers should be considered to identify challenges and opportunities in the effort toward achieving the overall goals (Jayathilake et al., 2021). Unfortunately, Iran does not have a national forest inventory program to determine how forest attributes, such as forest cover, volume stock, productivity, and resilience, have changed as a result of the new management policy associated with the FRP. Given the swift advancement and enhanced availability of remote sensing data, processing methods, and spatial analysis, it has become feasible to track forest changes and discern key factors impacting conversion, even in the absence of routine comprehensive inventory initiatives (Hu et al., 2022). Accurate forest LULCC tracking requires precise multi-temporal LULC mapping. This necessitates advanced processing to generate diverse spectral-temporal features representing various LULC categories (Pflugmacher et al., 2019). New developments, such as the Google Earth Engine (GEE) computing platform, methods for extracting features from time series, machine learning algorithms, and change detection models, may be integrated to facilitate large-scale forest LULCC monitoring (Nasiri et al., 2022). The results of LULCC monitoring can be interpreted using geospatial techniques and statistical models and integrated with other information to provide a deep understanding of forest cover dynamics.

Despite the importance of investigating the impact of FRP on HFs dynamics, the impact of deforestation drivers has been observed to vary across different regions (Meng et al., 2021; Sun et al., 2018), emphasizing the need for more comprehensive studies that take into account a broader range of influential drivers. Therefore, the purpose of this research is to use such tools to improve the understanding of the dynamics of the Iranian HFs, as complex systems influenced by conservation policies, climate change, human pressure, and the environmental conditions. Understanding the socioeconomic, climatic, and physiographic causes of forest cover change is critical for ecological restoration within the context of climate change and management practices (Meng et al., 2021). However, the relevance of such variables in the analysis of forest cover change drivers in Iran's HFs has not been quantified. This study evaluated the spatial and temporal trends of forest cover in Iran's HFs from 2010 to 2022 using remote sensing data, machine learning (ML) models, and statistical methodologies. The hypothesis of this study is that there have been substantial changes in the rates and trends of deforestation and forest recovery (here forest natural regeneration and FRP plan-based afforestation and forest restoration operations) following the implementation of the new conservation policy (FRP). We address the following research questions:

1. What areal changes have occurred between forest and other land-use classes following the implementation of the FRP?
2. How have the deforestation and forest recovery rates and trends in HFs been impacted by the FRP?
3. What are the dominant variables influencing deforestation and forest recovery in HFs when considering conservation policy, climate change, human activities, and the environmental conditions?
4. How has the FRP affected the factors that drive deforestation and forest recovery in HFs?

2. Materials and methods

2.1. Study area

The study area is located along the southern and southwestern coast of the Caspian Sea. The area stretches across three Iranian provinces, namely Gilan, Mazandaran, and Golestan (Fig. 1), with a total area of 58,700 km^2, and extends from 35°76′ to 38°45′N (latitude) and from

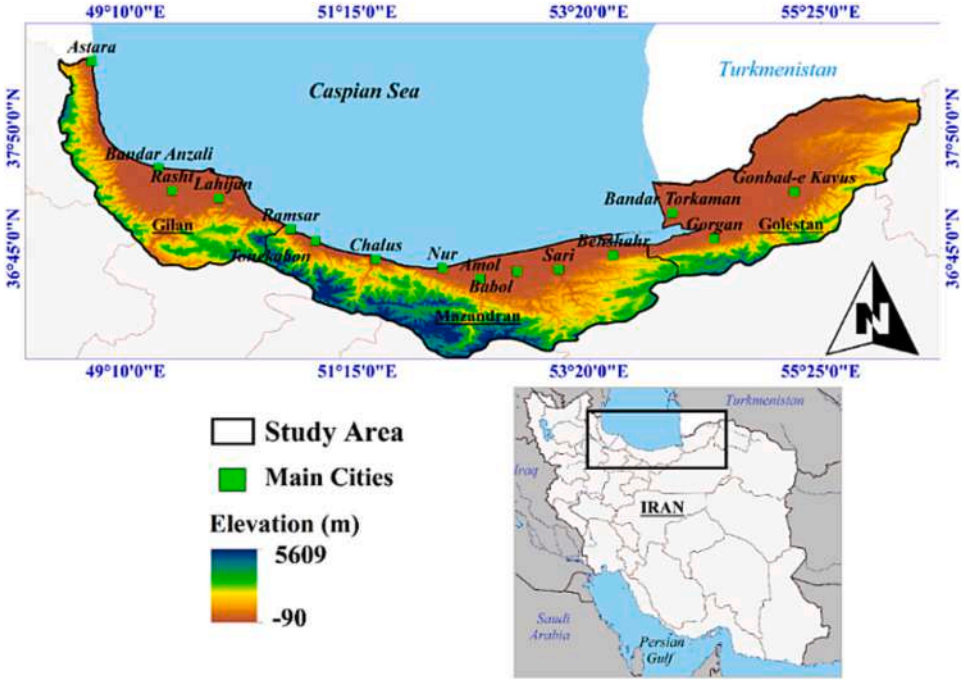

Fig. 1. Geographical location of the study area.

48°56′ to 56°30′E (longitude). The terrain of the region is mountainous, with minimum and maximum elevations ranging from 90 m below sea level in the coastal plains to 5609 m above sea level in the Alborz mountains (Mount Damavand). As one of the richest and most important biological hotspots in the world, the HFs are home to 80 woody plant species, 58 mammal species, and 180 bird species native to broadleaved temperate forests (Darvishsefat, 2006). The dominant tree species of the HFs are common hornbeam (*Carpinus betulus*), oriental beech (*Fagus orientalis*), Persian ironwood (*Parrotia persica*), and Caucasian oak (*Quercus macranthera*) (Nasiri et al., 2023). According to the Iranian population and housing census, in 2016 the study area was home to around 7,680,000 people.

Implemented in 2016, the RFP fully bans commercial exploitation of HFs. The FRP takes a comprehensive stance toward HF restoration, aligning with biodiversity preservation, soil-water conservation, ecotourism promotion, and sustainable development. Its measures curb commercial use, combat illegal cutting, and ensure sustained forest productivity. Yet, FRP faces challenges including illegal cutting, resource constraints, stakeholder awareness, competing interests, monitoring complexities, and the need for better collaboration (Panahi et al., 2021).

2.2. Methodology

Considering the research objectives, two time periods were defined to assess conversions between LULC classes: 2010–2016 (before FRP implementation) and 2016–2022 (after FRP implementation). The effect of new conservation policy on the processes of deforestation and forest recovery was investigated using multi-temporal LULC maps. By considering all possible LULCC drivers, i.e. climatic, physiographic, and

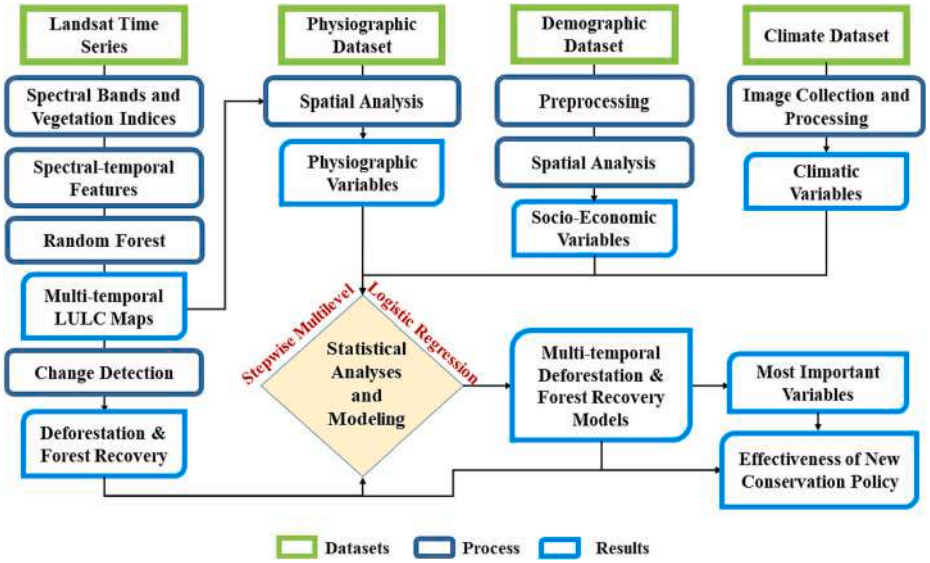

Fig. 2. The methodology used for monitoring and modeling HF cover dynamics.

demographic, and applying a modeling workflow, the most important drivers of forest cover change were identified (Fig. 2).

2.3. Data processing and analysis

2.3.1. Multi-temporal LULC maps

A multi-temporal reference dataset (training and validation samples) was created as the initial stage in LULC mapping. This dataset was developed by visually interpreting Google Earth (GE) very-high-resolution (VHR) satellite images, as well as a variety of natural, true, and false color composites derived from Landsat data. The most recent time point (i.e., 2022) served as the starting point for this process. A backward revision method was used for the other time points (2016, 2010) (Mas et al., 2016). The characteristics of the multi-temporal reference datasets are given in Table 1.

Feature extraction and LULC mapping were conducted utilizing Landsat time series and the GEE. This step encompassed several operations, including image collection and filtering, masking out clouds, calculating spectral indices, extracting spectral-temporal features, and performing image classification (Schulz et al., 2021). For all time points considered in this study, Landsat surface reflectance products (Level 2, Collection 2) have been collected in GEE between 1 March and 31 October of each year with a cloud cover <30% were used (Table 2). Since the majority of the HFs are dominated by deciduous trees, leaf-off (vs leaf-on) images were not considered in the image collections. The most commonly used vegetation indices (VIs) in LULC mapping (Tsai et al., 2018) were also calculated, i.e. the normalized difference vegetation index (NDVI), green normalized difference vegetation index (GNDVI), modified soil adjusted vegetation Index (MSAVI), and enhanced vegetation index (EVI). The spectral-temporal metrics (STMs) were calculated based on the per-pixel statistical values, including minimum, maximum, mean, standard deviation, and 25th, 50th, and 75th percentiles (Table 2). STMs are statistical metrics used to characterize the distribution of a spectral band or index across time (Pflugmacher et al., 2019). In addition to the STMs, Shuttle Radar Topography Mission (SRTM 1 Arc-Second Global) elevation data was used to generate elevation and slope layers (Pizarro et al., 2022).

The multi-temporal training samples (see 'multi-temporal LULC maps' section) were used to extract per-band pixel values of STMs (Table 2). The resulting spectral information was used to train the random forest (RF) model and generate multi-temporal LULC maps. RF is a classification ensemble learning approach that works by generating a large number of decision trees during training (Ho, 1995). RF modeling was selected over other machine learning (ML) approaches because RF models have been demonstrated to perform better in classifying LULC maps, but also based on their ability to effectively handle multi-modal data (Le Bris et al., 2015), the fact that they require fewer tuning parameters (Puissant et al., 2014), and their shorter processing time (Raczko and Zagajewski, 2017). Regarding hyperparameter tuning, only the number of trees (ntree) and the number of predictors (mtry) were tuned, while the default values were used for all other hyperparameters. This hyperparameter tuning was first done for the 2022 time point and optimal values (ntree = 500, mtry = 10) were then used to generate LULC maps for the other time points (2016 and 2010).

Table 1
Characteristics of the multi-temporal reference datasets (pixel resolution = 30 m).

LULC	Definition	No. of samples (training/validation)		
		2022	2016	2010
Forest (FO)	Natural and plantation forests with a patch area > 0.5 ha	5468/2373	5684/2436	5936/2544
Grassland (GR)	Pastures and meadows	4234/1812	4225/1810	4204/1801
Cropland (CR)	Rainfed and irrigated farmlands, all fruit trees	7038/3015	7002/3001	6988/2994
Built-up area (BA)	Urban and industrial areas, and roads	4180/1800	4151/1780	4116/1734
Barren land (BL)	Sandy areas, beaches, and mines	3754/1620	3690/1582	3605/1544
Water body (WB)	Rivers and lakes	2646/1134	2646/1134	2646/1134

Table 2
Multi-temporal satellite images and spectral-temporal metrics (STMs) used for land-use/land-cover (LULC) classification. Each STM was calculated for six bands and four vegetation indices (VIs). (10 spectral bands and VIs × 7 STMs = 70, and two topographic layers).

Time point	Landsat mission	No. of images	STMs	No. of features
2022	L-9	84	Minimum, maximum, mean, standard deviation, and 25th, 50th, and 75th percentiles	72
2016	L-8	78		
2010	L-5	49		

2.3.2. LULCC, deforestation, and forest recovery modeling

A post-classification change detection method was used to detail information regarding the temporal dynamics of HFs and their mutual exchanges with other LULC classes. The spatial patterns of pixels transformed from/into forests were generated based on the resulting LULCC data, and a third polynomial model was fitted to identify the intensity of deforestation and forest recovery across the study area.

2.3.3. Explanatory variable selection

To model the dynamics of deforestation (forest loss) and forest recovery (forest gain), variables were used that are frequently included in LULCC process (Table 3). These variables could cover the socioeconomic, climatic, and physiographic aspects of the LULC change process.

2.3.3.1. Demographic variables. Demographic variables included in this study were population growth rate, population density, the ratio of urban to rural population, and the ratio of the land consumption rate to the population growth rate (LCRPGR; (Verburg et al., 1999). The LCRPGR was used to assess sustainable land use while accounting for competing forces such as urbanization and population increase (Calka et al., 2022). Based on census data from the years 2006 and 2016, the population size for the target time points (2010, 2016, and 2022) and the population growth rate were estimated using the following two equations:

$$P_n = P_0\,(1+r)^n \tag{1}$$

$$r = \frac{ln\left(\frac{P_n}{P_0}\right)}{n} \tag{2}$$

where P_n is the population size at time point (year) n, P_0 is the population size at time point (year) 0, and n is the difference between two time points (in years). r is the population growth rate and ln is the natural logarithm. Population density was determined by dividing each town's population by its area (number of people per square kilometer). In order to calculate the urban-to-rural population ratio, the urban population was first calculated as the difference between the total population and the rural population. Then we used the urban and rural populations to compute this ratio at the town scale. Two elements must be defined to estimate LCRPGR: land consumption rate (LCR), which in this study was calculated using multi-temporal LULC maps, and the population growth rate, which was calculated as described above. LCRPGR can be defined as:

$$LCRPGR = \frac{Land\ Consumption\ Rate\ (LCR)}{Population\ Growth\ Rate} \tag{3}$$

Table 3
Variables used in the modeling of deforestation and forest recovery.

Variable	Reason for inclusion	Year	Source	References
Elevation (m)	Accessibility and suitability for agricultural activities	Static	SRTM[a] digital elevation model	Zeng et al. (2021)
Aspect (degree)		Static		Beygi Heidarlou et al. (2020)
Slope (degree)		Static		Beygi Heidarlou et al. (2020)
Ratio of urban to rural population	Shifting of rural populations to urban areas or vice versa; a proxy for urban development or agricultural development	2010 and 2016	Census data	Ehrhardt-Martinez et al. (2002)
Population growth rate (%)	Human pressure on land	2010 and 2016		DeFries et al. (2010)
Population density (per km$^{2)}$		2010 and 2016		Kummer and Turner (1994)
LCRPGR[b]		2010 and 2016	Census data, LULC maps, and township boundaries	Gilani et al. (2020)
Distance to built-up areas (m)	Accessibility and human pressure on land	2010 and 2016	LULC maps	Armenteras et al. (2013)
Distance to cropland edges (m)		2010 and 2016		Wijaya et al. (2015)
Distance to the road network (m)		2010 and 2016		Barber et al. (2014)
Distance to the coastline (m)	Accessibility and suitability for built-up development	Static	National Cartographic Center (NCC) of Iran	Taylor et al. (2022)
Distance to rivers (m)	Accessibility and suitability for agricultural activities	2010 and 2016		Bax et al. (2016)
Cropland density	High values for a given LULC class in areas with high density	2010 and 2016	LULC maps	Tayyebi and Pijanowski (2014); Tayyebi et al. (2014)
Forest density		2010 and 2016		
Rangeland density		2010 and 2016		
Built-up area density		2010 and 2016		Beygi Heidarlou et al. (2020)
Land surface temperature (°C)	Suitability for agricultural activities and built-up development	2010–2016 2016–2022	MOD11A2.006 Terra land surface temperature data	Sinha and Swaminathan (1991)
Mean precipitation (mm)	Suitability for agricultural activities	2010–2016 2016–2022	ERA5-Land monthly averaged precipitation data	Hoyos et al. (2013)

[a] . Shuttle Radar Topography Mission digital elevation model.
[b] . Land consumption rate to the population growth rate.

$$LCR = \frac{ln\left(\frac{Urb_n}{Urb_0}\right)}{n} \quad (4)$$

The socio-economic variables were calculated at the town scale (3 provinces, 42 towns). Finally, all the values (population growth rate, population density, and LCRPGR LCRC population) were imported to township boundaries to generate raster layers.

2.3.3.2. Climatic variables. As the climatic variables, satellite-derived temperature and precipitation datasets were used to calculate mean land surface temperature (LST) and mean precipitation for the two time periods representing before and after FRP implementation (2010–2016 and 2016–2022). For precipitation, ERA5-Land monthly averaged data (https://developers.google.com/earth-engine/datasets/catalog/ECMWF_ERA5_LAND_MONTHLY) with a spatial resolution of 9 km was used. Temperature was calculated using the MOD11A2.006 Terra land surface temperature data (https://developers.google.com/earth-engine/datasets/catalog/MODIS_006_MOD11A2) with a temporal resolution of 8 days and a spatial resolution of 1 km. All the processes described above, including image collection and mean calculation, were done in the GEE.

2.3.3.3. Physiographic variables. The topographic, distance, and density-based variables such as elevation, slope, aspect, and distance to the road network, to built-up areas, to cropland edges, to rivers, and to the coastline were created based on Euclidean distances and corresponding layers. The Shuttle Radar Topography Mission (SRTM) digital elevation model was used for topographic layers, while distance-based variables were generated based on LULC maps. Density-based variables were produced in ArcGIS v.10.5 based on LULC maps and focal statistic and density toolset. Finally, all the layers were resampled to 30 m spatial resolution using the bilinear interpolation method.

2.4. Statistical analyses and deforestation/forest recovery modeling

To analyze the relationships between forest loss/gain, FRP implementation, and the associated key variables in deforestation and forest recovery in the study area, a binary logistic regression (LR) model was employed to accommodate data gathered at different scales. In a first phase, a binary LR model was created to estimate the likelihood of forest loss/gain at the pixel level between 2010 and 2016 (before FRP implementation) and between 2016 and 2022 (after FRP implementation of the FRP). For this purpose, the dependent binary variable (either forest loss or gain) was assigned to 0 if the pixel showed a positive or negative change and to 1 for pixels showing no change. Environmental, demographic, and socio-economic variables that were shown to be substantially connected with forest cover dynamics were included in the LR as explanatory variables.

In addition, to avoid multicollinearity, all explanatory variables were first incorporated into the LR models for each time period, and Spearman coefficients for independent (explanatory) variables were obtained. When two or more independent variables have a significant correlation with each other, this is referred to as multicollinearity. This effect makes determining the unique influence of each independent variable on the dependent variable challenging (Alin, 2010). The correlation coefficient (r) can have values ranging from -1 to $+1$, and a correlation coefficient (r) of >0.8 or > 0.9 between two variables is regarded to indicate complete collinearity. Furthermore, the tolerance value (varies from 0 to 1) and variance inflation factor (VIF) were used to calculate multicollinearity. When the tolerance value is <0.25, it suggests that there is little multicollinearity. A VIF values >4 or > 10 are frequently seen as indicating multicollinearity. The correlation coefficient, tolerance, and VIF are defined as follows:

$$r = \frac{\sum(x_i - \bar{x})(y_i - \bar{y})}{\sqrt{\sum (x_i - \bar{x})^2 \sum (y_i - \bar{y})^2}} \quad (5)$$

$$Tolerance = 1 - R^2 \quad (6)$$

$$VIF = \frac{1}{Tolerance} \quad (7)$$

where r is the correlation coefficient, x_i and y_i are the x- and y-variable values, $\bar{x}$ and $\bar{y}$ are means of the x- and y-variable values, and R^2 is the unadjusted coefficient.

To reduce any spatial autocorrelation effects, 2450 pixels were randomly selected across the study area, with a minimum sampling distance of 1 km. The residuals of the response variable were tested for spatial autocorrelation using the global Moran's index. The Global Moran's Index is a statistical metric employed to evaluate spatial autocorrelation within a dataset by analyzing the presence of similarity or dissimilarity patterns among neighboring observations (Anselin, 1995). Moran's index values in general range from +1 to −1. Values of +1 and − 1 denote complete positive and negative spatial autocorrelation, respectively, whereas 0 denotes perfect spatial randomness. Moran's index was calculated to be 0.0007 for the periods 2010–2016 and 2016–2022, indicating that there was no spatial autocorrelation between the selected time periods.

The cell values corresponding to each random point's dependent and explanatory variables were then retrieved, and stepwise backward LR models were implemented in XLStat 2019 (Addinsoft, Paris, France). The likelihood of forest loss and gain was calculated for all selected pixels in the study area using the coefficients from these LR models. In addition, model performance (2010–2016 and 2016–2022) was assessed using the relative operating characteristic (ROC). The ROC curve is a statistical tool used to assess the performance of binary models, representing the trade-off between true positive rate and false positive rate across different threshold settings. An ideal model would have an ROC curve that reaches the top left corner, indicating high sensitivity and low false positive rate. The area under the ROC curve (AUC-ROC) is a measure of the overall performance of the model, with a higher value indicating better classification ability to differentiate between positive and negative instances (Bradley, 1997). For this analysis, the full set of data points utilized in the LR analysis of the study area was divided into points for training (70%) and points for validation (30%). The ROC curve is defined as a plot of the false-positive (FP) rate (1-specificity) on the x-axis and the true-positive (TP) rate (the sensitivity) on the y-axis, derived using the following equations:

$$X = 1 - specificity = 1 - \left[\frac{True\ negative}{Tru\ negative + False\ positive}\right] \quad (8)$$

$$Y = Sensitivity = \lceil\frac{True\ negative}{True\ positive + False\ negative}\rceil \quad (9)$$

3. Results

3.1. Land-use land-cover mapping

The accuracy assessment of the LULC maps yielded overall accuracy ranging from 87.61% to 89.69% (Table S1). The corresponding LULC maps are illustrated in Fig. 3.

3.2. LULC change detection statistics

Fig. 4 presents statistics on the extent of LULC classes derived from multi-temporal LULC maps. Generally, forests, grasslands, barren lands, and water bodies decreased. In contrast, croplands and built-up area experienced an increasing trend throughout the study period. Also, please refer to Fig. S1 in the supplementary material, which displays net land use and land cover changes during the study period.

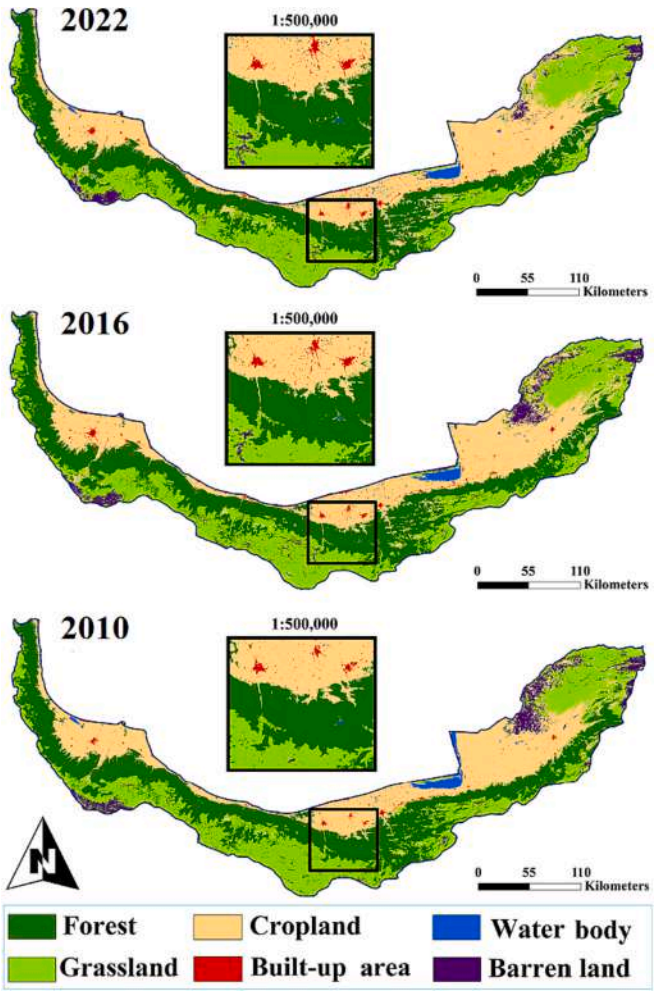

Fig. 3. Multi-temporal LULC maps extracted from Landsat time series.

Based on the results from 2010 to 2016, prior to the implementation of the FRP, the areas of forests, grasslands, barren lands, and water bodies decreased by over 90,514, 8190, 15,204, and 17,566 ha, respectively. In contrast, croplands and built-up areas increased by 105,222 and 26,252 ha, respectively. In the period after FRP implementation (2016 to 2022), LULC changes resulted in decreases in forests, grasslands, barren lands, and water bodies by 26,887, 12,482, 36,069, and 232 ha, respectively. As in the years before FRP implementation, croplands and built-up areas experienced an increase, by 62,308 and 13,362 ha, respectively (Table 5).

3.3. Deforestation/forest recovery

We observed a remarkable decline in the deforestation rate between the two time periods. (Fig. 5). Specifically, 144,803 ha and 88,075 ha of forest were changed into other LULC classes before and after FRP, respectively. Moreover, the forest recovery rate was higher in the period after FRP (61,191 ha) than in the earlier period (54,289 ha). As described in the Methods, our study site is comprised of the three provinces Gilan, Mazandaran, and Golestan, with different levels of development and population density. Therefore, we additionally analyzed LULCC for each of these provinces separately (Table S2).

Over the periods both before and after FRP, the deforestation process mainly involved the expansion of croplands, grasslands, and barren lands (Fig. 6), with the transformation of forest to barren land increasing considerably in the second period (2016–2022). Additionally, following

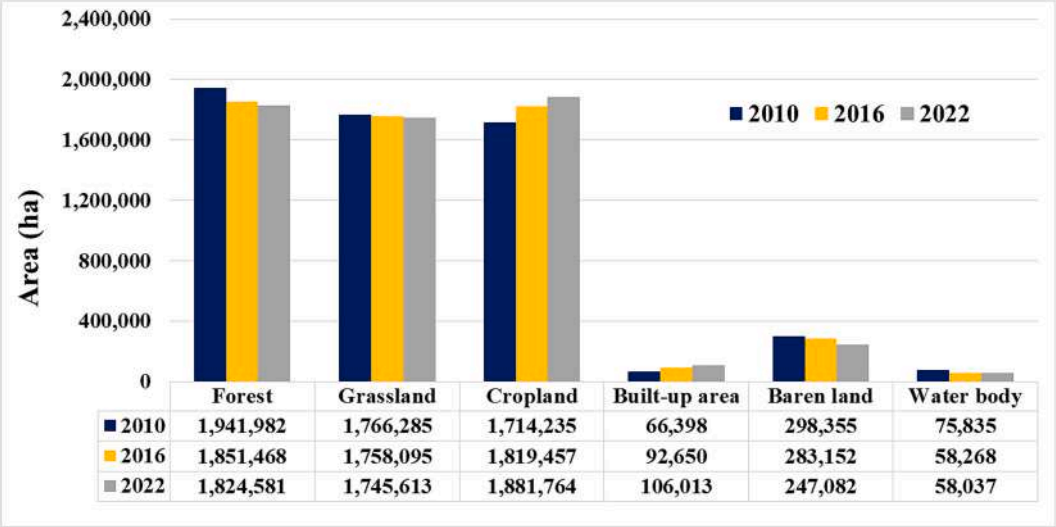

Fig. 4. The extent of the different LULC classes at different time points (all numbers are rounded to full hectares).

Table 5
LULC changes before (2010–2016) and after (2016–2022) implementation of the Forest Rest Plan (FRP) in the study area. All values are rounded to full hectares.

	Change 2010–2016			Change 2016–2022		
	Area change (ha)	Proportion of the total change (%)	Annual change (ha)	Area change (ha)	Proportion of the total change (%)	Annual change (ha)
Forest	−90,514	−68.8	−15,085	−26,887	−35.5	−4481
Grassland	−8190	−6.2	−1365	−12,482	−16.5	−2080
Cropland	105,222	80.0	17,537	62,308	82.3	10,385
Built-up area	26,252	20.0	4375	13,362	17.7	2227
Barren land	−15,204	−11.6	−2534	−36,069	−47.7	−6012
Water body	−17,566	−13.4	−2928	−232	−0.3	−38.6

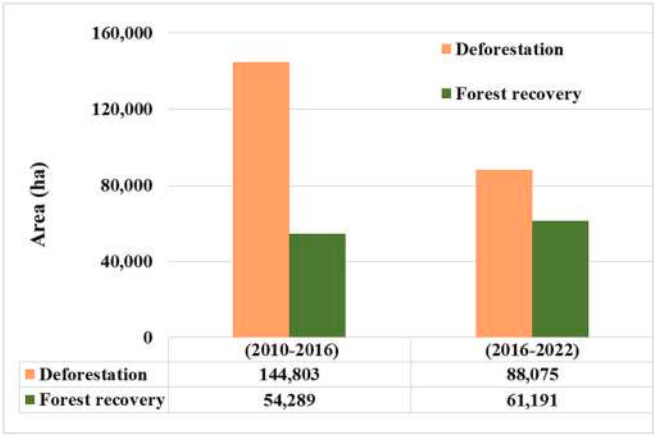

Fig. 5. Statistics on deforestation and forest recovery before (2010–2016) and after (2016–2022) implementation of the Forest Rest Plan (FRP). All values are rounded to full hectares.

implementation of the FRP, there was a marked decrease in the transformation of forest to cropland (53.80% vs. 43.56%) and an increase in the transformation of forest to grassland (39.82% vs. 46.34%). Moreover, over both periods the main pattern of forest recovery was the transformation of cropland and grassland into forests.

Fig. 7 depicts the spatial trend of deforestation and forest recovery before and after FRP, where pixels with higher values indicate more intense deforestation or forest recovery. According to these findings, the deforestation intensity declined whereas the forest recovery intensity rose in the second period (2016–2022). The most intense deforestation occurred in Mazandaran province, closely followed by Gilan and Golestan. Forest recovery intensity differed widely among the provinces, with most recovery occurring in Gilan.

3.4. Deforestation/forest recovery modeling

The derived correlation matrices (Table S3), tolerance values, and VIF values revealed that no effects of multicollinearity were predicted in the LR forest loss and forest gain models before (2010–2016) and after (2016–2022) FRP. Based on these results, the all LR models for 2010–2016 and 2016–2022 were significant (Table 6).

At the pixel level, stepwise multilevel LR models showed that the ratio of urban to rural population, cropland density, forest density, rangeland density, built-up area density, mean precipitation, and land surface temperature (LST) were statistically significant ($P < 0.05$) in the forest loss models before and after FRP implementation. Additionally, after FRP implementation, variables such as distance to road network, elevation, and slope were also found to be statistically significant ($P < 0.05$) in the forest loss model (Table 7). Both before and after FRP, rangeland density was the most significant driver of forest loss ($\chi^2 = 218.52$, $\chi^2 = 149.12$), followed by cropland density ($\chi^2 = 116.06$, $\chi^2 = 28.50$) and forest density ($\chi^2 = 30.36$, $\chi^2 = 18.67$).

Variables that significantly influenced forest gain before FRP included elevation, slope, ratio of urban to rural population, population density, distance to road network, cropland density, forest density, rangeland density, LST, and mean precipitation. Apart from slope, the same variables, along with the distance to rivers, were the most statistically significant ($P < 0.05$) criteria after FRP implementation. Among these, the most influential variables both before and after FRP implementation were rangeland density ($\chi^2 = 214.82$, $\chi^2 = 153.28$), cropland density ($\chi^2 = 127.35$, $\chi^2 = 48.99$), and forest density ($\chi^2 = 27.14$, $\chi^2 = 33.48$; Table 8). The negative values for the β coefficient for each

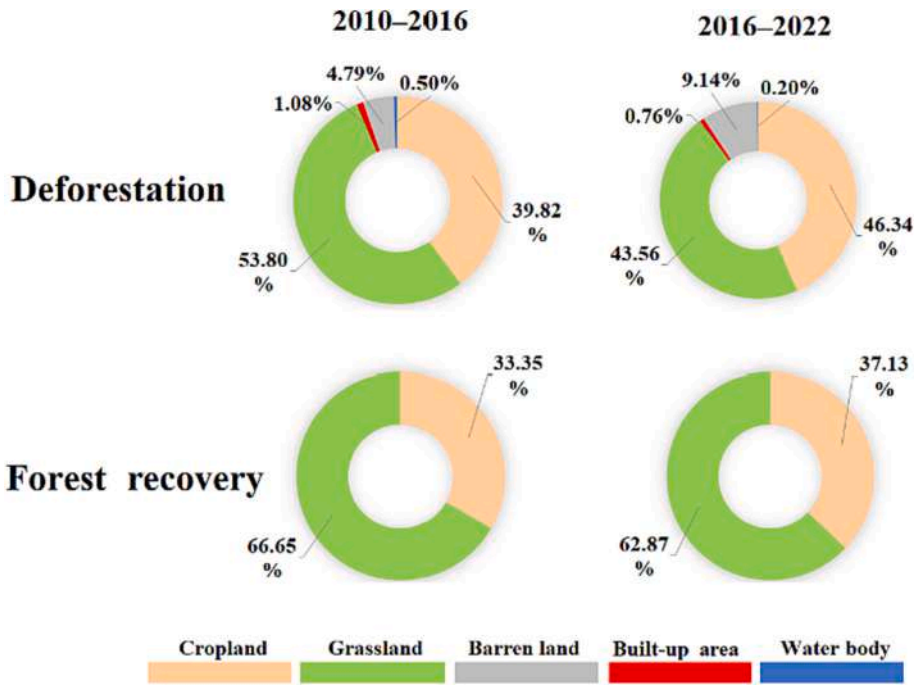

Fig. 6. Contribution of each LULC class to deforestation and forest recovery before and after implementation of the Forest Rest Plan (FRP).

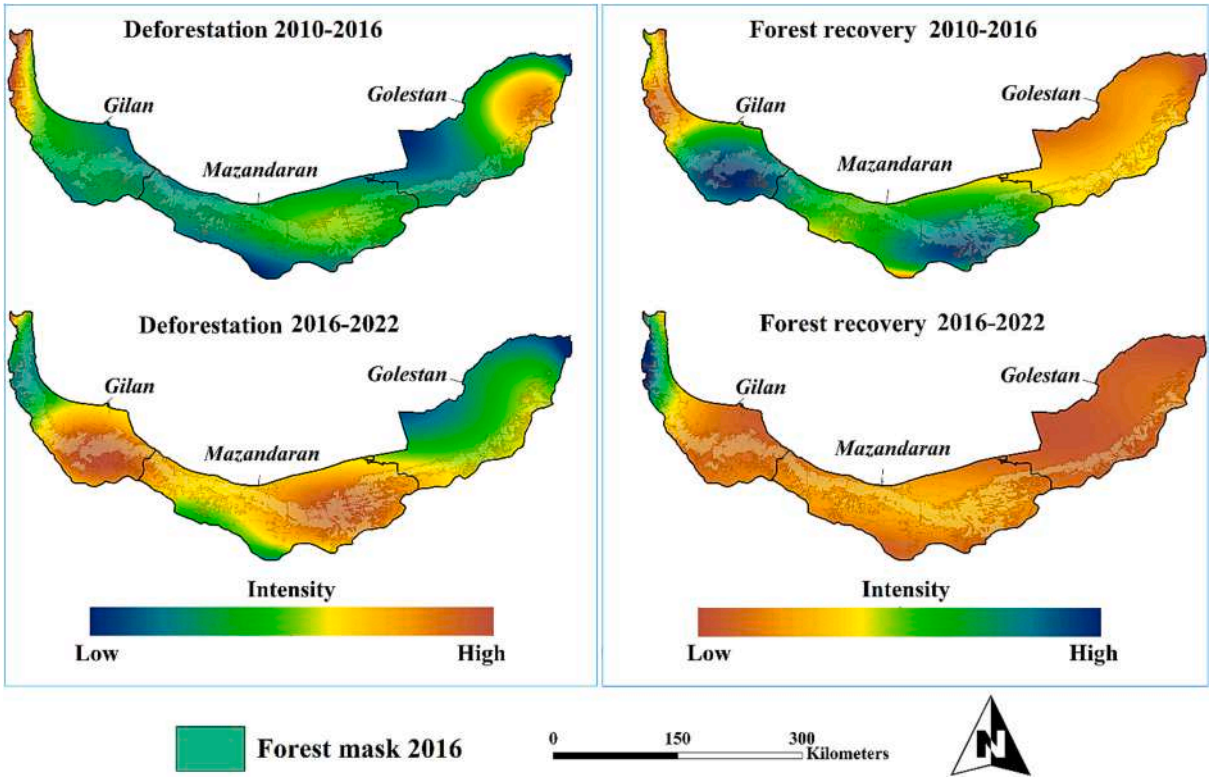

Fig. 7. Spatial trends of deforestation and forest recovery based on multi-temporal LULC maps.

variable demonstrate that the likelihood of forest loss or gain increased in direct proportion to the reduction in value from these factors.

Fig. 8 shows the ROC curves and the area under the ROC curves (AUC) before (2010–2016) and after (2016–2022) FRP implementation for training and validation data. These findings support the appropriate goodness of fit of the LR models, indicating adequate accuracy for the studied time periods in HFs.

4. Discussion

One of the most significant issues faced by Iran's Natural Resources and Watershed Management Organization before 2016 was the continuance of forest logging (implementation of approved forestry plans) vs. forest rest (also called National Forest Breathing Project) (Heidari and Karamdoost Maryan, 2017). There are two opposing perspectives on

Table 6
Overall LR model results for HFs in the studied time periods.

		Forest loss		Forest gain	
		2010–2016	2016–2022	2010–2016	2016–2022
−2 Log(likelihood)	Chi^2	714.60	375.37	670.27	371.14
	$Pr > Chi^2$	< 0.0001	< 0.0001	< 0.0001	< 0.0001
Goodness of fit	R^2 (Nagelkerke)	0.49	0.31	0.47	0.31

Table 7
Coefficients of the pixel-based forest loss model before (2010–2016) and after (2016–2022) implementation of the Forest Rest Plan (FRP). Bold fonts indicate statistically significant effects ($P < 0.05$).

Variable	β coefficient		Standard error		Wald Chi^2		$Pr > Chi^2$	
	Before FRP	After FRP	Before FRP	After FRP	Before FRP	After FRP	Before FRP	After FRP
Intercept	18.76	23.75	11.91	11.63	2.48	4.17	0.115	0.041
Elevation	0.00	0.00	0.00	0.00	1.95	22.76	0.162	**< 0.0001**
Aspect	0.00	0.00	0.00	0.00				
Slope	0.01	0.01	0.01	0.01	3.00	4.31	0.083	**0.038**
Ratio of urban to rural population	−0.02	0.02	0.01	0.01	12.08	14.64	**0.001**	**0.000**
Population growth rate	−0.08	0.00	0.06	0.00	1.91		0.167	
Population density	−0.00	0.00	0.00	0.00	2.17	13.78	0.141	**0.000**
LCRPGR[a]	0.00	0.02	0.00	0.01		2.83		0.093
Distance to built-up areas	0.00	0.00	0.00	0.00	2.10		0.148	
Distance to cropland edges	0.00	0.00	0.00	0.00				
Distance to coastline	0.00	0.00	0.00	0.00	3.64	1.85	0.056	0.174
Distance to road network	0.00	0.00	0.00	0.00		14.22		**0.000**
Distance to rivers	0.00	0.00	0.00	0.00	2.42		0.120	
Cropland density	6.63	3.27	0.62	0.61	116.06	28.50	**< 0.0001**	**< 0.0001**
Forest density	2.97	2.25	0.54	0.52	30.36	18.67	**< 0.0001**	**< 0.0001**
Rangeland density	7.63	5.89	0.52	0.48	218.52	149.12	**< 0.0001**	**< 0.0001**
Built-up area density	3.80	−10.52	1.40	6.55	7.31	2.58	**0.007**	**0.108**
Land surface temperature	−0.08	−0.10	0.04	0.04	4.19	6.68	**0.041**	**0.010**
Mean precipitation	262.17	227.50	92.46	99.90	8.04	5.19	**0.005**	**0.023**

[a] . Land consumption rate to the population growth rate.

Table 8
Coefficients of the pixel-based forest gain model before (2010–2016) and after (2016–2022) implementation of the Forest Rest Plan (FRP). Bold fonts indicate statistically significant effects ($P < 0.05$).

Variable	β coefficient	Standard error		Wald Chi^2		$Pr > Chi^2$	
	Before FRP	After FRP	Before FRP	After FRP	Before FRP	After FRP	Before FRP	After FRP
Intercept	−24.42	−36.29	11.78	12.13	4.30	8.95	0.038	0.003
Elevation	0.00	0.00	0.00	0.00	6.04	23.55	**0.014**	**< 0.0001**
Aspect	0.00	0.00	0.00	0.00				
Slope	−0.03	−0.01	0.01	0.01	12.10	2.96	**0.001**	0.085
Ratio of urban to rural population	0.03	−0.02	0.01	0.01	25.97	6.39	**< 0.0001**	**0.011**
Population growth rate	0.00	0.00	0.00	0.00				
Population density	0.00	−0.00	0.00	0.00	14.34	7.77	**0.000**	**0.005**
LCRPGR[a]	0.00	−0.02	0.00	0.01		1.64		0.200
Distance to built-up areas	0.00	0.00	0.00	0.00		3.34		0.068
Distance to cropland edges	0.00	0.00	0.00	0.00	2.82		0.093	
Distance to coastline	0.00	0.00	0.00	0.00		1.89		0.169
Distance to road network	0.00	0.00	0.00	0.00	2.75	5.98	**0.097**	**0.014**
Distance to rivers	0.00	0.00	0.00	0.00		5.18		**0.023**
Cropland density	−6.86	−4.71	0.61	0.67	127.35	48.99	**< 0.0001**	**< 0.0001**
Forest density	−2.67	−3.27	0.51	0.56	27.14	33.48	**< 0.0001**	**< 0.0001**
Rangeland density	−7.18	−6.66	0.49	0.54	214.82	153.28	**< 0.0001**	**< 0.0001**
Built-up area density	0.00	0.00	0.00	0.00				
Land surface temperature	0.10	0.15	0.04	0.04	6.46	13.44	**0.011**	**0.000**
Mean precipitation	−229.20	−358.79	63.06	101.59	13.21	12.47	**0.000**	**0.000**

[a] . Land consumption rate to the population growth rate.

sustainable forest logging and FRP. For years, it has been demonstrated that, while harvested forests are less resistant and resilient to disturbances (Chiarucci and Piovesan, 2020; Curtis et al., 2018), the main strength of the forest logging technique is that it improves the dynamics and stability of the forest, while the main weakness is damage to forest reproduction, loss of biodiversity, and significant habitat fragmentation (Chakraborty et al., 2017; Do et al., 2022). At the same time, forest exploitation creates jobs on a national and regional scale (Hejazyan and Lotfalian, 2015). The most significant advantage of FRP, on the other hand, is the reduction of soil erosion, while its main drawback is an increase in wood smuggling in poorly monitored areas, for instance forests at high elevations and on steep slopes, and in regions with high population density (Table 7).

Contrasting processes at the landscape level in HFs, as revealed by LULCC analysis in this study, and their relationship to explanatory variables reflect the complex interactions between different

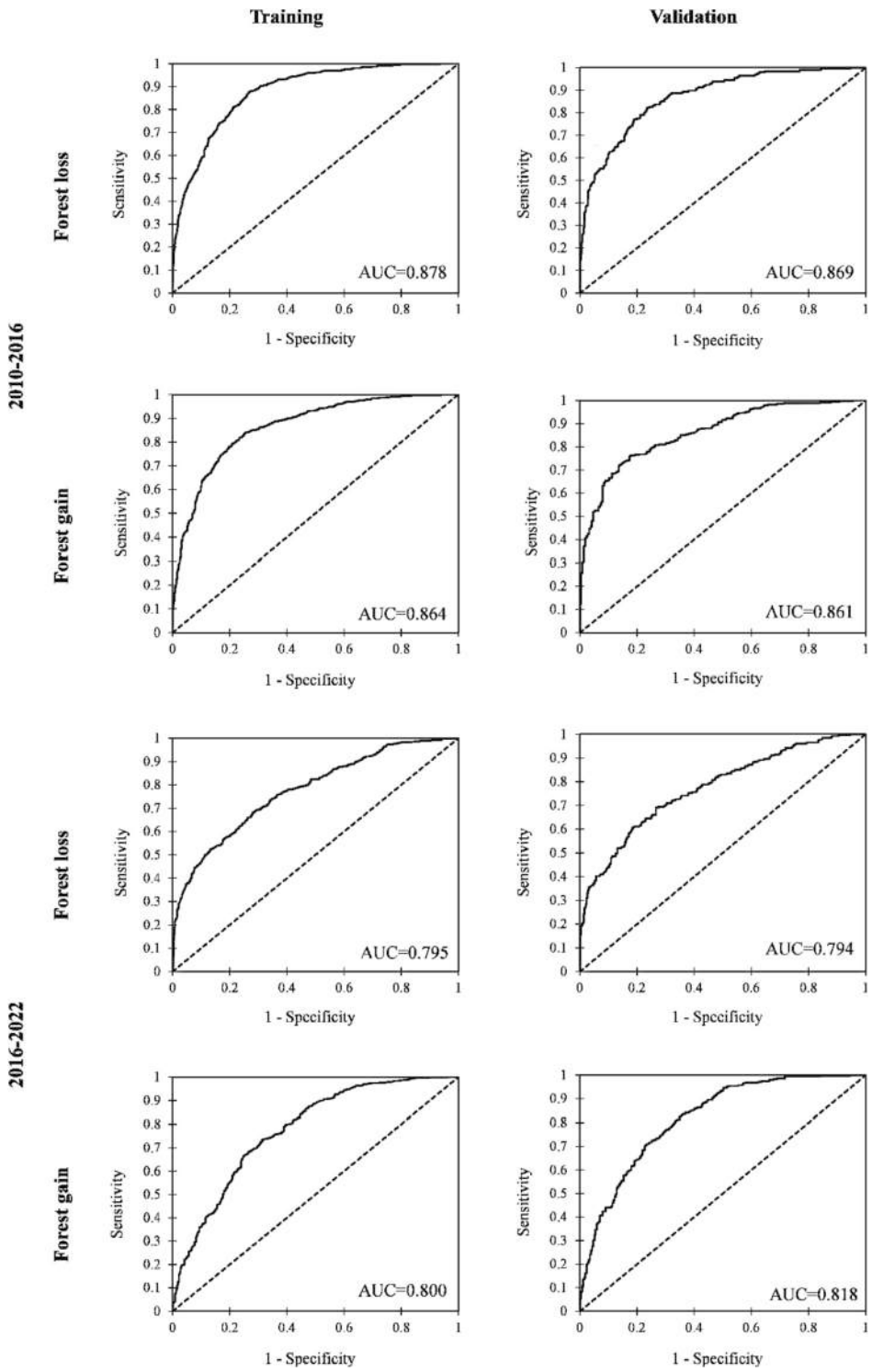

Fig. 8. Relative operating characteristic (ROC) curves of different LR models. The area under the ROC curve (AUC) value is given for each curve.

characteristics of the land that occur at multiple spatial and temporal scales in these coupled human and natural systems (Viedma et al., 2006). Our findings demonstrate that the major LULCC pathway in HFs can be summarized as deforestation for residential areas and for cropland and rangeland development, which is typical for forest frontier regions (Fig. 6). These inclinations encourage the further formation of productive land (i.e. deforestation and the construction of pastures for livestock [mostly cattle and sheep] and new agricultural land), as well as the sale and privatization of forest areas to build residential areas, especially extensive bungalow constructions. Livestock raising and pasture development in HFs, in particular, have experienced tremendous expansion in recent years; while the activity has not been demonstrated to be significant for a family's economy, it is viewed as a means of providing the financial resources essential for their livelihood. Prior to the implementation of the FRP, a scheme dubbed livestock removal from the HFs was carried out, which – according to many studies – was not successful (Motamed and Ghorbani Piralidehi, 2021). It is worth mentioning that the government's FRP programs for

monitoring and preventing pasture and livestock expansion have grown considerably since the policy was enacted (Heidari and Karamdoost Maryan, 2017).

Between 2010 and 2022, a total of 117,401 ha of HFs (Hyrcanian Forests) were destroyed (Fig. 4). According to a study conducted by Shooshtari and Gholamalifard (2015), the most significant drivers of deforestation in this region are the conversion of natural forest stands into croplands, rangelands, and built-up areas. Our findings indicate that, among the factors considered in the HFs, the implementation of the FRP had a significant relationship with forest gain in these forests. Despite the establishment of the FRP in HFs in 2016, deforestation is still occurring. With the adoption of the FRP in HFs after this year, annual forest cover change decreased to 4481 ha between 2016 and 2022 (Table 5).

The results regarding forest recovery, on the other hand, showed an increase in forest area by 61,191 ha after FRP implementation. This significant increase demonstrates that government engagement, in the form of logging restrictions and monitoring efforts to prevent illegal logging, aided forest recovery to some extent. Apparently, the laws enacted within the framework of the FRP to prevent tree cutting and logging of HFs, as well as those regarding the use of land and natural resources (i.e. forest cover change to other land uses), have halted deforestation activities. Furthermore, by enacting stronger restrictions limiting the growth of residential areas and agricultural land uses in the provinces covered by HFs, Iran's national forest services have been able to prevent forests loss and promote forest recovery. Cultural traditions, religious beliefs, and some pre-existing conservation policies connected to values placed on certain forest types may also contribute to forest conservation in traditional and local communities of HFs.

In line with the findings, the most severe forest degradation occurred in discrete forest fragments. These sites were in proximity to both forested and non-forested lands. Some other researchers have reported similar findings (Beygi Heidarlou et al., 2020; Vogelmann et al., 2017). Increasing the distance from the road network, rough terrain, steep slopes, and a lack of proper access also leads to further degradation of forest areas owing to a decline in monitoring by the Iranian Forestry Organization. Additional causes contributing to the region's deforestation include the expansion of built-up areas and croplands, the construction of new roads, the need for water supplies, and high population growth and density, with the most influential factors varying by location (Beygi Heidarlou et al., 2020).

According to the findings of LR modeling from 2010 to 2016 (before implementation of the FRP), the most influential factors for forest loss were rangeland density, cropland density, forest density, ratio of urban to rural population, built-up area density, mean precipitation, and LST. However, following the implementation of the FRP, other criteria were identified as being important for forest loss in the region, including elevation, slope, and population density (Table 7). After the war between Iraq and Iran (1980–1988), an intense building phase began in Iran in 1989, resulting in significant changes throughout the nation (Sarmadi and Badri, 2017). Following this time, deforestation activities intensified, due to the availability of non-standard roads that were previously utilized for farmland extension and rehabilitation and for the development of built-up regions (Baumann et al., 2015). According to Abdullah and Nakagoshi (2006), locations with a large population and better accessibility (low elevation and slope) and also agricultural operations are frequently the key driving forces in landscape dynamics. Vu et al. (2014) reported that it is difficult for humans to obtain resources from forest areas located on steep slopes or in highlands or to convert them to pastures and croplands. Because of the availability of marginal agricultural land in HFs, the majority of the damage occurred there, reflecting the significance of human activity in deforestation. Other major sources of forest degradation in the region include livestock grazing (capable of changing the composition of vegetation), tourist attractions, local people's use of forests for food and firewood, illicit logging, expansion of cultivated land, and periodic floods (Poorzady and Bakhtiari, 2009). Furthermore, this region (i.e. HFs and the three provinces they covered) has been the focus of development and tourism activities in Iran, due to its good weather, fertile land, job prospects, industrial growth, and national railway accessibility (Shooshtari and Gholamalifard, 2015).

As mentioned in the previous section, human activities are the main drivers that can influence the implementation of the FRP and generate significant uncertainties about the future. In other words, the long-term sustainability of the HFs depends on these drivers. Although the implementation of the FRP has a profoundly positive impact on the SFM of HFs, its effectiveness relies on robust governance structures, stakeholder engagement, and the continuous evaluation and adaptation of policies based on local contexts and evolving challenges. For instance, several policy changes and measures are required to combat deforestation and forest degradation at the local and provincial levels. Enhancing monitoring and surveillance systems is crucial for detecting and preventing illegal logging and encroachments. This may involve investing in technology, training forest rangers, and promoting collaboration between government agencies, law enforcement, and local communities. Additionally, enacting and enforcing robust laws and regulations that prohibit illegal logging, encroachments, and unsustainable land-use practices are essential. Moreover, sustainable agriculture and responsible mining practices have the potential to alleviate pressure on forests. Policy interventions, such as offering tax incentives, subsidies, and technical support to landowners who embrace sustainable practices, can facilitate this transition. Also, the integration of the FRP with the establishment of well-managed protected areas forms a cohesive and comprehensive approach to countering deforestation and forest degradation, ultimately fostering the sustainable utilization and preservation of HFs.

Climate change presents significant uncertainties for the FRP. According to Kiapasha et al. (2017), the impacts of rising temperatures and shifting precipitation patterns in the HFs raise concerns about reforestation success and the adaptability of chosen tree species to future climates. Moreover, these climate-induced shifts influence soil health and nutrient cycling, potentially resulting in diminished soil function and fertility, which in turn affects overall plant growth and regeneration potential. Furthermore, climate change may lead to shifts in species distribution, as some species migrate or expand into new habitats, potentially upsetting existing ecosystem dynamics and competition relationships. Phenological changes, potentially disrupting pollinator interactions, coupled with climate-induced shifts in the growing season (EOS), could further disrupt ecological synchrony, impacting forest regeneration and the efficacy of the FRP. Additionally, the heightened frequency of wildfires (Nami et al., 2018), storms (Jahani and Saffariha, 2021), and pest outbreaks (Babaie Kafaky et al., 2022) due to climate change poses a threat, damaging restored forests and undermining FRP objectives. Dry spells compound these challenges by inducing water stress, hindering germination, exacerbating seedling vulnerability, intensifying competition with invasive species, delaying growth, heightening susceptibility to disease, altering plant dynamics, and potentially undermining the attainment of FRP goals.

5. Conclusion

The main aim of this study was to gain a deeper knowledge of the interactions between the new conservation policy (FRP), climatic change, human pressure, and environmental conditions on the dynamics of the Iranian HFs. From the methodology and results, the following conclusions can be drawn. Landsat time series, GEE-based cloud computing, spectral-temporal features, and machine learning algorithms such as RF provide opportunities for large-scale forest cover monitoring. Our study additionally confirms that the spatial analysis tools and stepwise multiple logistic regression applied here are reliable for precisely modeling deforestation and forest recovery dynamics. The fundamental hypothesis of this study was supported by the results,

which showed that significant changes in deforestation and forest recovery rates and trends have occurred as a result of the implementation of the new conservation policy (FRP). The effectiveness of the new conservation policy (FRP) was also confirmed by the findings, which showed that while deforestation continued after FRP implementation, the annual change in forest cover decreased and the intensity of forest recovery increased slightly. To increase the efficiency of FRP, more monitoring efforts to prevent illegal logging and trading, as well as enhanced afforestation and agroforestry activities, are needed. Moreover, the establishment of adaptation, preventative, and restorative activities by decision-makers and planners seems absolutely essential to prevent further deforestation caused by climate change, human pressure, and other drivers. To address these challenges and prevent further land loss, natural resource managers must consider social, biological, and environmental factors specific to each area. Government support is crucial in helping communities transition from using fuel wood to alternative fuels. Creating local job opportunities and promoting awareness about ecosystem services through education can curb deforestation. Designating protected areas conserves biodiversity and curbs destructive activities like logging and mining. Additionally, paying for ecosystem services offers financial rewards to landowners who preserve natural benefits such as clean water, carbon storage, and biodiversity. This approach aligns economic incentives with conservation, fostering sustainable land use. In the modern, continually developing world with a variety of stakeholders involved and declining resource availability, studies like the one presented here are a valuable step forward in preparing real-time and precise information for conservation and management of the environment and for the long-term maintenance of ecosystem services.

Declaration of Competing Interest

The authors declare no conflict of interest.

Data availability

Data will be made available on request.

Acknowledgement

We thank Melissa Dawes for help editing the manuscript.

Appendix A. Supplementary data

Supplementary data to this article can be found online at https://doi.org/10.1016/j.ecoinf.2023.102351.

References

Abdullah, S.A., Nakagoshi, N., 2006. Changes in landscape spatial pattern in the highly developing state of Selangor, peninsular Malaysia. Landsc. Urban Plan. 77, 263–275.
Ahmad, A., Ahmad, S., Nabi, G., Liu, Q.-J., Islam, N., Luan, X., 2022. Trends in deforestation as a response to management regimes and policy intervention in the Hindu Kush Himalaya of Pakistan. Front. Environ. Sci. 125.
Alin, A., 2010. Multicollinearity. In: Wiley Interdisciplinary Reviews: Computational Statistics, 2, pp. 370–374.
Anselin, L., 1995. Local indicators of spatial association—LISA. Geogr. Anal. 27, 93–115.
Armenteras, D., Cabrera, E., Rodríguez, N., Retana, J., 2013. National and regional determinants of tropical deforestation in Colombia. Reg. Environ. Chang. 13, 1181–1193.
Babaie Kafaky, S., Kiadaliri, H., Mataji, A., Akhavan, R., Hodjati, S., 2022. Assessment of ecological capability and decline of Quercus castaneifolia CAM habitat in Hyrcanian forests (case study: Savadkooh). Int. J. Environ. Sci. Technol. 1–14.
Barber, C.P., Cochrane, M.A., Souza Jr., C.M., Laurance, W.F., 2014. Roads, deforestation, and the mitigating effect of protected areas in the Amazon. Biol. Conserv. 177, 203–209.
Başkent, E.Z., 2021. Assessment and valuation of key ecosystem services provided by two forest ecosystems in Turkey. J. Environ. Manag. 285, 112135.
Baumann, M., Radeloff, V.C., Avedian, V., Kuemmerle, T., 2015. Land-use change in the Caucasus during and after the Nagorno-Karabakh conflict. Reg. Environ. Chang. 15, 1703–1716.
Bax, V., Francesconi, W., Quintero, M., 2016. Spatial modeling of deforestation processes in the central Peruvian Amazon. J. Nat. Conserv. 29, 79–88.
Beygi Heidarlou, H., Shafiei, A.B., Erfanian, M., Tayyebi, A., Alijanpour, A., 2020. Underlying driving forces of forest cover changes due to the implementation of preservation policies in Iranian northern Zagros forests. Int. For. Rev. 22, 241–256.
Beygi Heidarlou, H., Banj Shafiei, A., Nasiri, V., Niţă, M.D., Borz, S.A., Lopez-Carr, D., 2023. Impact of Iran's Forest nationalization law on Forest cover changes over six decades: a case study of a Zagros sparse coppice oak Forest. Sensors 23, 871.
Bradley, A.P., 1997. The use of the area under the ROC curve in the evaluation of machine learning algorithms. Pattern Recogn. 30, 1145–1159.
Calka, B., Orych, A., Bielecka, E., Mozuriunaite, S., 2022. The ratio of the land consumption rate to the population growth rate: a framework for the achievement of the spatiotemporal pattern in Poland and Lithuania. Remote Sens. 14, 1074.
Chakraborty, A., Ghosh, A., Sachdeva, K., Joshi, P.K., 2017. Characterizing fragmentation trends of the Himalayan forests in the Kumaon region of Uttarakhand, India. Eco. Inform. 38, 95–109.
Chiarucci, A., Piovesan, G., 2020. Need for a global map of forest naturalness for a sustainable future. Conserv. Biol. 34, 368–372.
Coops, N.C., Tompalski, P., Goodbody, T.R., Achim, A., Mulverhill, C., 2023. Framework for near real-time forest inventory using multi source remote sensing data. Forestry 96, 1–19.
Curtis, P.G., Slay, C.M., Harris, N.L., Tyukavina, A., Hansen, M.C., 2018. Classifying drivers of global forest loss. Science 361, 1108–1111.
Darvishsefat, A.A., 2006. Atlas of Protected Areas of Iran. University of Tehran, Tehran.
DeFries, R.S., Rudel, T., Uriarte, M., Hansen, M., 2010. Deforestation driven by urban population growth and agricultural trade in the twenty-first century. Nat. Geosci. 3, 178–181.
Do, A.N.T., Tran, H.D., Ashley, M., Nguyen, A.T., 2022. Monitoring landscape fragmentation and aboveground biomass estimation in can Gio mangrove biosphere reserve over the past 20 years. Eco. Inform. 70, 101743.
Ehrhardt-Martinez, K., Crenshaw, E.M., Jenkins, J.C., 2002. Deforestation and the environmental Kuznets curve: a cross-national investigation of intervening mechanisms. Soc. Sci. Q. 83, 226–243.
Fischer, K.M., Project, I.I.N.R.M., 2010. Study on Timber Harvesting Ban in NWFP, Pakistan. Intercooperation Pakistan.
Gilani, H., Ahmad, S., Qazi, W.A., Abubakar, S.M., Khalid, M., 2020. Monitoring of urban landscape ecology dynamics of Islamabad capital territory (ICT), Pakistan, over four decades (1976–2016). Land 9, 123.
Hassan, M.M., Duveneck, M., Southworth, J., 2023. The role of the refugee crises in driving forest cover change and fragmentation in Teknaf, Bangladesh. Ecol. Inf. 74, 101966.
Heidari, M., Karamdoost Maryan, B., 2017. The study and policy cessation of forest utilization or forest logging in Hyrcanian forests (case study: Shafarood forests). Iran. J. Forest Pop. Res. 24, 724–736.
Hejazyan, M., Lotfalian, M., 2015. The consequences of non-normative reduce the volume of wood harvested from forests in the north of Iran. J. Forest Range 105, 70–75.
Ho, T.K., 1995. Random decision forests. In: Proceedings of 3rd International Conference on Document Analysis and Recognition. IEEE, pp. 278–282.
Hoyos, L.E., Cingolani, A.M., Zak, M.R., Vaieretti, M.V., Gorla, D.E., Cabido, M.R., 2013. Deforestation and precipitation patterns in the arid C haco forests of central a rgentina. Appl. Veg. Sci. 16, 260–271.
Hu, L., Shariff, A.R.B.M., Omar, H., Song, D.-X., Wu, H., 2022. GEE-Based Spatiotemporal Evolution of Deforestation Monitoring in Malaysia and its Drivers, Remote Sensing Application: Regional Perspectives in Agriculture and Forestry. Springer, pp. 279–302.
Jahani, A., Saffariha, M., 2021. Modeling of trees failure under windstorm in harvested Hyrcanian forests using machine learning techniques. Sci. Rep. 11, 1124.
Jayathilake, H.M., Prescott, G.W., Carrasco, L.R., Rao, M., Symes, W.S., 2021. Drivers of deforestation and degradation for 28 tropical conservation landscapes. Ambio 50, 215–228.
Jourgholami, M., Majnounian, B., 2011. Harvesting systems in Hyrcanian forest, Iran; limitations and approaches. In: The Forest Engineering Network. Formec, Austria, pp. 9–13.
Kiapasha, K., Darvishsefat, A., Zargham, N., Julien, Y., Sobrino, J., Nadi, M., 2017. Shifts of start and end of season in response to air temperature variation based on Gimms dataset in Hyrcanian forests. Int. Arch. Photogramm. Remote. Sens. Spat. Inf. Sci. 42, 155–160.
Kummer, D.M., Turner, B.L., 1994. The human causes of deforestation in Southeast Asia. Bioscience 44, 323–328.
Le Bris, A., Chehata, N., Briottet, X., Paparoditis, N., 2015. A random forest class memberships based wrapper band selection criterion: application to hyperspectral. In: 2015 IEEE International Geoscience and Remote Sensing Symposium (IGARSS). IEEE, pp. 1112–1115.
Lynch, J., Maslin, M., Balzter, H., Sweeting, M., 2013. Choose satellites to monitor deforestation. Nature 496, 293–294.
Mas, J.-F., Lemoine-Rodríguez, R., Taud, H., 2016. Toward a near-real time forest monitoring system. Investig, Geogr. 168–175.
Meng, Y., Yang, M., Liu, S., Mou, Y., Peng, C., Zhou, X., 2021. Quantitative assessment of the importance of bio-physical drivers of land cover change based on a random forest method. Eco. Inform. 61, 101204.
Morley, P.J., Donoghue, D.N., Chen, J.-C., Jump, A.S., 2018. Integrating remote sensing and demography for more efficient and effective assessment of changing mountain forest distribution. Eco. Inform. 43, 106–115.

Motamed, M.K., Ghorbani Piralidehi, F., 2021. Challenges of advancing sericulture as a sustainable income generating rural activity in Guilan province. Geogr. Stud. Coast. Areas J. 2, 5–24.
Nami, M., Jaafari, A., Fallah, M., Nabiuni, S., 2018. Spatial prediction of wildfire probability in the Hyrcanian ecoregion using evidential belief function model and GIS. Int. J. Environ. Sci. Technol. 15, 373–384.
Nasiri, V., Sadeghi, S.M.M., Moradi, F., Afshari, S., Deljouei, A., Griess, V.C., Maftei, C., Borz, S.A., 2022. The influence of data density and integration on Forest canopy cover mapping using Sentinel-1 and Sentinel-2 time series in Mediterranean oak forests. ISPRS Int. J. Geo Inf. 11, 423.
Nasiri, V., Beloiu, M., Darvishsefat, A.A., Griess, V.C., Maftei, C., Waser, L.T., 2023. Mapping tree species composition in a Caspian temperate mixed forest based on spectral-temporal metrics and machine learning. Int. J. Appl. Earth Obs. Geoinf. 116, 103154.
Panahi, P., Jamzad, Z., Jalili, A., Talebi, K.S., Pourhashemi, M., 2021. The role of the National Botanical Garden of Iran in ex situ conservation of Buxus hyrcana Pojark.; An endangered species. Urban For. Urban Green. 57, 126951.
Pflugmacher, D., Rabe, A., Peters, M., Hostert, P., 2019. Mapping pan-European land cover using Landsat spectral-temporal metrics and the European LUCAS survey. Remote Sens. Environ. 221, 583–595.
Pizarro, S.E., Pricope, N.G., Vargas-Machuca, D., Huanca, O., Ñaupari, J., 2022. Mapping land cover types for Highland Andean ecosystems in Peru using Google earth engine. Remote Sens. 14, 1562.
Poorzady, M., Bakhtiari, F., 2009. Spatial and temporal changes of Hyrcanian forest in Iran. iForest-Biogeosci. Forest. 2, 198.
Puissant, A., Rougier, S., Stumpf, A., 2014. Object-oriented mapping of urban trees using random Forest classifiers. Int. J. Appl. Earth Obs. Geoinf. 26, 235–245.
Raczko, E., Zagajewski, B., 2017. Comparison of support vector machine, random forest and neural network classifiers for tree species classification on airborne hyperspectral APEX images. Eur. J. Remote Sensing 50, 144–154.
Rahmanian, S., Pourghasemi, H.R., Pouyan, S., Karami, S., 2021. Habitat potential modelling and mapping of Teucrium polium using machine learning techniques. Environ. Monit. Assess. 193, 1–21.
Santos, Y.L., Yanai, A.M., Ramos, C.J., Graça, P.M., Veiga, J.A., Correia, F.W., Fearnside, P.M., 2022. Amazon deforestation and urban expansion: simulating future growth in the Manaus metropolitan region, Brazil. J. Environ. Manag. 304, 114279.
Sarmadi, H., Badri, M., 2017. The effect of Hashemi Rafsanjani's technocrat government and changing of foreign policy of Iran from power to pragmatism. Acad. J. Educ. Res. 5, 29–33.
Schulz, D., Yin, H., Tischbein, B., Verleysdonk, S., Adamou, R., Kumar, N., 2021. Land use mapping using Sentinel-1 and Sentinel-2 time series in a heterogeneous landscape in Niger, Sahel. ISPRS J. Photogramm. Remote Sens. 178, 97–111.
Scullion, J.J., Vogt, K.A., Drahota, B., Winkler-Schor, S., Lyons, M., 2019. Conserving the last great forests: a meta-analysis review of the drivers of intact forest loss and the strategies and policies to save them. Front. Forests Glob. Change 2, 62.
Shooshtari, S.J., Gholamalifard, M., 2015. Scenario-based land cover change modeling and its implications for landscape pattern analysis in the Neka Watershed, Iran. Remote Sensing Appl.: Soc. Environ. 1, 1–19.
Silva Junior, C.H.L., Pessôa, A.C.M., Carvalho, N.S., Reis, J.B.C., Anderson, L.O., Aragão, L.E.O.C., 2021. The Amazon's deforestation rate in 2020 is projected to be the greatest of the decade Nat. Nat. Ecol. Evol. 5, 144–145.
Sinha, S., Swaminathan, M., 1991. Deforestation, climate change and sustainable nutrition security: a case study of India. Clim. Chang. 19, 201–209.
Sotirov, M., Pokorny, B., Kleinschmit, D., Kanowski, P., 2020. International forest governance and policy: institutional architecture and pathways of influence in global sustainability. Sustainability 12, 7010.
Stritih, A., Bebi, P., Rossi, C., Grêt-Regamey, A., 2021. Addressing disturbance risk to mountain forest ecosystem services. J. Environ. Manag. 296, 113188.
Sun, Z., Wang, X., Yamamoto, H., Tani, H., Zhong, G., Yin, S., Guo, E., 2018. Spatial pattern of GPP variations in terrestrial ecosystems and its drivers: climatic factors, CO2 concentration and land-cover change, 1982–2015. Eco. Inform. 46, 156–165.
Taylor, C.M., Klein, C., Parker, D.J., Gerard, F., Semeena, V.S., Barton, E.J., Harris, B.L., 2022. "Late-stage" deforestation enhances storm trends in coastal West Africa. Proc. Natl. Acad. Sci. 119, e2109285119.
Tayyebi, A., Pijanowski, B.C., 2014. Modeling multiple land use changes using ANN, CART and MARS: comparing tradeoffs in goodness of fit and explanatory power of data mining tools. Int. J. Appl. Earth Obs. Geoinf. 28, 102–116.
Tayyebi, A.H., Tayyebi, A., Khanna, N., 2014. Assessing uncertainty dimensions in land-use change models: using swap and multiplicative error models for injecting attribute and positional errors in spatial data. Int. J. Remote Sens. 35, 149–170.
Tong, X., Brandt, M., Yue, Y., Ciais, P., Rudbeck Jepsen, M., Penuelas, J., Wigneron, J.-P., Xiao, X., Song, X.-P., Horion, S., 2020. Forest management in southern China generates short term extensive carbon sequestration. Nat. Commun. 11, 129.
Tsai, Y.H., Stow, D., Chen, H.L., Lewison, R., An, L., Shi, L., 2018. Mapping vegetation and land use types in Fanjingshan National Nature Reserve using google earth engine. Remote Sens. 10, 927.
Verburg, P.H., De Koning, G., Kok, K., Veldkamp, A., Bouma, J., 1999. A spatial explicit allocation procedure for modelling the pattern of land use change based upon actual land use. Ecol. Model. 116, 45–61.
Viedma, O., Moreno, J.M., Rieiro, I., 2006. Interactions between land use/land cover change, forest fires and landscape structure in sierra de Gredos (Central Spain). Environ. Conserv. 33, 212–222.
Vogelmann, J.E., Khoa, P.V., Lan, D.X., Shermeyer, J., Shi, H., Wimberly, M.C., Duong, H.T., Huong, L.V., 2017. Assessment of forest degradation in Vietnam using landsat time series data. Forests 8, 238.
Vu, Q.M., Le, Q.B., Frossard, E., Vlek, P.L., 2014. Socio-economic and biophysical determinants of land degradation in Vietnam: An integrated causal analysis at the national level. Land Use Policy 36, 605–617.
Wijaya, P.A., Saleh, M.B., Tiryana, T., 2015. Spatial model of deforestation in Jambi Province for the periode 1990–2011. Jurnal Manajemen Hutan Tropika 21, 128–137.
Yuh, Y.G., Tracz, W., Matthews, H.D., Turner, S.E., 2023. Application of machine learning approaches for land cover monitoring in northern Cameroon. Eco. Inform. 74, 101955.
Zeng, Z., Wang, D., Yang, L., Wu, J., Ziegler, A.D., Liu, M., Ciais, P., Searchinger, T.D., Yang, Z.-L., Chen, D., 2021. Deforestation-induced warming over tropical mountain regions regulated by elevation. Nat. Geosci. 14, 23–29.